# Chains of Magnetosomes Extracted from AMB-1 Magnetotactic Bacteria for Application in Alternative Magnetic Field Cancer Therapy

**Edouard Alphandéry,[†,‡,*] Stéphanie Faure,[‡] Olivier Seksek,[§] François Guyot,[†,⊥] and Imène Chebbi[‡]**

[†]Institut de Minéralogie et de Physique des Milieux Condensés, Université Pierre et Marie Curie, 4 Place Jussieu, 75005, Paris, France, [‡]Nanobacterie SARL, 36 Boulevard Flandrin, 75016, Paris, France, [§]Laboratoire ANbioPhy-Fre 3207, Université Pierre et Marie Curie, 4 Place Jussieu, 75005, Paris, France, and [⊥]Institut de Physique du Globe de Paris, Université Paris Diderot, Sorbonne Paris Cité, 1 Rue Jussieu, 75005, Paris, France

**ABSTRACT** Chains of magnetosomes extracted from AMB-1 magnetotactic bacteria are shown to be highly efficient for cancer therapy when they are exposed to an alternative magnetic field. When a suspension containing MDA-MB-231 breast cancer cells was incubated in the presence of various amounts of extracted chains of magnetosomes, the viability of these cells remained high in the absence of an alternative magnetic field. By contrast, when this suspension was exposed to an alternative magnetic field of frequency 183 kHz and field strengths of 20, 40, or 60 mT, up to 100% of these cells were destroyed. The antitumoral activity of the extracted chains of magnetosomes is demonstrated further by showing that they can be used to fully eradicate a tumor xenografted under the skin of a mouse. For that, a suspension containing ~1 mg of extracted chains of magnetosomes was administered within the tumor and the mouse was exposed to three heat cycles of 20 min, during which the tumor temperature was raised to ~43 °C. We also demonstrate the higher efficiency of the extracted chains of magnetosomes compared with various other materials, *i.e.*, whole inactive magnetotactic bacteria, individual magnetosomes not organized in chains, and two different types of chemically synthesized superparamagnetic iron oxide nanoparticles currently tested for alternative magnetic field cancer therapy. The higher efficiency of the extracted chains of magnetosomes compared with that of the other nanoparticles is attributed to three factors: (i) a specific absorption rate higher for the magnetosomes than for the chemically synthesized superparamagnetic iron oxide nanoparticles, (ii) a more uniform heating for the chains of magnetosomes than for the individual magnetosomes and (iii) the ability of the chains of magnetosomes to penetrate within the cancer cells or bind at the cell membrane following the application of the alternative magnetic field, which enables efficient cell destruction. Biodistribution studies revealed that extracted chains of magnetosomes administered directly within xenografted breast tumors progressively left the tumors during the 14 days following their administration and were then eliminated in large proportion in the feces.

**KEYWORDS:** nanotechnology · chains of magnetosomes · magnetic hyperthermia · alternative magnetic field · cancer · thermotherapy · magnetotactic bacteria · biodistribution of ferromagnetic nanoparticles · magnetosome · tumor

Our concept should favor the emergence of a new generation of therapeutical substance which may be considered as a drug or a medical device depending on medical regulation, the way in which it is used and its behavior in the organism. It relies on the idea that the movement, the activation, and the detection of such substance could be controlled externally by a medical device. This approach is of special interest in the field of cancer research since an efficient treatment with limited side effects would require the use of a substance that could be sent specifically within the cancer cells, that could be monitored in the organism, for example to verify that the substance is located within the tumor before the treatment is started, and that could be activated on demand by a medical device. A good candidate for such a substance would be magnetic iron oxide nanoparticles. These nanoparticles may indeed potentially be guided within the cancer cells using a magnetic field, detected using magnetic resonance imaging (MRI) and heated by being exposed to an alternative magnetic field (AMF).[1] In this case, the destruction or elimination of tumors would occur by increasing the tumor temperature typically within the range 37−45 °C for hyperthermia[2] or above 45 °C for thermoablation.[3] In previous work, heating has been induced using chemically synthesized nanoparticles, mainly in the form of superparamagnetic iron oxide nanoparticles (SPION), which were either mixed in solution or mixed with cells or administered to a living organism.[1−16] The efficiency of this type of thermotherapy has been demonstrated on several types of cancers including brain cancer,[8,9] prostate cancer,[10−13] and breast cancer.[14−16] Research in this area has also led to industrial developments. In addition to the company Nanobacterie, which led to this study, there are at least three companies that develop cancer therapy using the heat generated by magnetic nanoparticles when the latter are exposed to an AMF.[17] The patents that have been published by these

* Address correspondence to edouardalphandery@hotmail.com.

Received for review April 7, 2011 and accepted July 6, 2011.

**Published online July 06, 2011**
10.1021/nn201290k

companies describe various ways of using the heat generated by chemically synthesized magnetic nanoparticles to carry out AMF cancer therapy.[18]

Although significant progress has been made in the area of nanoparticle cancer therapy, concerns have been raised regarding the toxicity induced by the presence of the chemically synthesized nanoparticles in the body. In order to minimize the potential side effects arising during the clinical treatments, the quantity of nanoparticles administered needs to be as small as possible while still retaining the desired effect. For that, magnetic nanoparticles have to generate a sufficiently large amount of heat; that is, they must yield significant specific absorption rates (SAR). Therefore, there is a need for magnetic nanoparticles having a higher heating capacity than that usually obtained with chemically synthesized nanoparticles. This will be useful to reduce the amount of magnetic material needed to heat a biological tissue or cell. This can be achieved by using nanoparticles with either large volumes or high magnetocrystalline anisotropy.[19] In part due to their large volumes, the magnetosomes synthesized by magnetotactic bacteria[20,21,22] produce a larger amount of heat than the chemically synthesized nanoparticles when they are exposed to an alternative magnetic field. This has been shown for bacterial magnetosomes mixed in solution, which were either contained within the magnetotactic bacteria or extracted from these bacteria, and for magnetosomes arranged in chains or forming individual nanoparticles.[19,23,24] Another advantage of the magnetosomes *versus* chemically synthesized nanoparticles comes from the presence of a phospholipid membrane surrounding them, which could favor the binding of an anticancerous agent or of an antibody to them. The presence of these molecules at the magnetosome surface could be used either to carry out chemotherapy in combination with hyperthermia or to target the tumor, which is an essential step if the magnetosomes are administered intravenously. Finally, it has been reported that the magnetosomes are not particularly toxic when they are injected in rats.[25,26] This suggests that there is no major hurdle for the development of a cancer thermotherapy that uses bacterial magnetosomes as heating sources. Among the different types of bacterial magnetosomes, those arranged in chains and extracted from the magnetotactic bacteria seem to be the best candidate for thermotherapy since they are not prone to aggregation but are presumably sufficiently close to each other to yield a high *in vivo* heating efficiency.

In this article, the heating efficiency and antitumoral activity of chains of magnetosomes extracted from magnetotactic bacteria are compared with those of individual magnetosomes detached from the chains by heat and sodium-dodecyl-sulfate (SDS) treatments as well as with those contained within whole inactive magnetotactic bacteria. The impact of the length of the chains of magnetosomes on the efficiency of the therapy is also studied by treating mice with two different types of chains of magnetosomes of different lengths. Moreover, the efficiency of the extracted chains of magnetosomes is compared with that of two different types of SPION (SPION@Citrate and SPION@PEG), which are currently being tested for AMF cancer therapy.[27] The parameters used to carry out the different treatments such as the frequency and strength of the applied magnetic field, the treatment duration, or the number of times that the treatment is repeated are typical of those currently tested for AMF cancer therapy.[2−19]

## RESULTS AND DISCUSSION

**Nanoparticles.** Six different types of nanoparticles were used as heating sources: whole inactive magnetotactic bacteria; chains of magnetosomes extracted from magnetotactic bacteria of standard length ~150 nm, designated as Ch-Std; chains of magnetosomes extracted from magnetotactic bacteria of longer length (~300 nm) than that of the Ch-Std, designated as Ch-EDTA; individual magnetosomes, ~45 nm in mean size, detached from the extracted chains of magnetosomes by heat and SDS treatments, designated as IM; superparamagnetic iron oxide nanoparticles less than 20 nm in size, stable in water, coated with either citrate ions (SPION@Citrate) or PEG molecules (SPION@PEG). The magnetosomes contained within the bacteria, the Ch-Std and Ch-EDTA, are held together by biologic material,[28] whereas this material has been mostly removed in the IM.[29] These different types of magnetosomes are essentially made of maghemite.[30] They are well-crystallized monodomain nanoparticles with a ferromagnetic behavior at physiological temperature. The SPION@Citrate and SPION@PEG are also made of maghemite, but due to their smaller sizes than the magnetosomes, they are superparamagnetic at physiological temperature. The magnetization curves of the whole inactive bacteria, Ch-Std, SPION@Citrate, and SPION@PEG are presented elsewhere.[30−32] The magnetization curves of the IM and Ch-EDTA are similar to that of the Ch-Std. The transmission electron microscopy (TEM) micrographs of three suspensions containing whole magnetotactic bacteria, Ch-Std, and IM deposited on top of a carbon-coated copper grid are shown in Figure 1a−c, respectively. Figure 1a shows that a typical magnetotactic bacterium contains several chains of magnetosomes, while Figure 1b and c show that the Ch-Std distribute more homogeneously within the carbon grid than the IM, which are prone to aggregation. Nanoparticle characteristics, preparation methods, and the methods used to measure the concentrations of the different suspensions of nanoparticles are described in more detail in the Materials and Methods section.

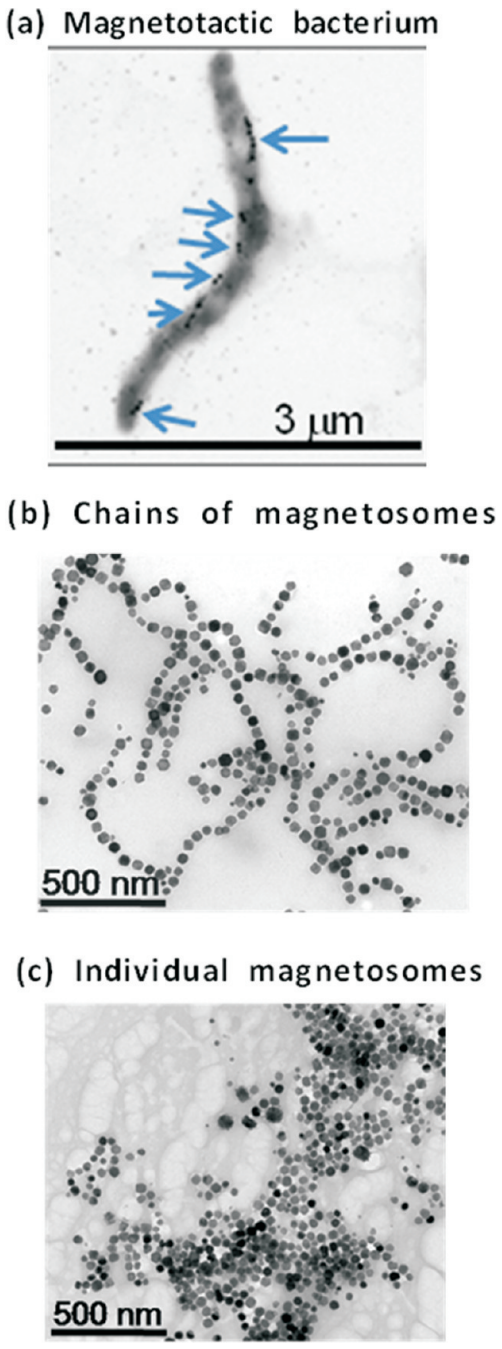


**Figure 1. (a) Transmission electron microscopy micrograph of one cell of *Magnetospirillum magneticum* strain AMB-1, where the arrows indicate the localization of the chains of magnetosomes; (b) TEM micrograph of the chains of magnetosomes extracted from the bacteria; (c) TEM micrograph of individual magnetosomes detached from the chains by heat and SDS treatments.**

**Determination of the Magnetic Field Strength That Can Heat MDA-MB-231 Cells Incubated in the Presence of the Ch-Std.** MDA-MB-231 cells were first seeded on Petri dishes (diameter of 30 mm with 50 000 cells per Petri dish) and grew during 24 h. They were then immediately mixed with the Ch-Std and exposed to an alternating magnetic field of frequency 183 kHz and strength ~20, ~ 40, or ~60 mT during 20 min. The temperature was measured with a thermocouple microprobe (IT-18, Physitemp, Clifton, NJ, USA), which measures the temperature macroscopically, *i.e.*, the temperature of the cell suspension as a whole and not the temperature within each individual cell. Figure 2a shows that when the suspension containing the cells and the Ch-Std is exposed to the AMF of strength 20 mT, the temperature of the suspension does not increase. By contrast, when this suspension is exposed to an AMF of strength ~40 mT, Figure 2b shows that the temperature of the suspension increases and the magnitude of this increase, $\Delta T$, increases with the concentration of Ch-Std incubated from $\Delta T = 2$ °C for a concentration of Ch-Std of 0.125 or 0.25 mg/mL up to $\Delta T = 4-6$ °C for a concentration of Ch-Std of 0.5 or 1 mg/mL (Figure 2b). Figure 2c shows that when the cells are incubated in the presence of various concentrations of Ch-Std and exposed to an AMF of 60 mT during 20 min, the temperature increases by 15 to 16 °C for a concentration of Ch-Std incubated lying between 0.125 and 1 mg/mL. This temperature increase is relatively similar to that of 14 °C observed for the cells incubated in the absence of Ch-Std, indicating that this temperature increase mainly arises from the Foucault's currents, *i.e.*, from the heat produced by the ions contained in the suspension and not from that produced by the Ch-Std. The heating due to Foucault's currents, which is potentially toxic, occurs at high magnetic field strength, in agreement with a previous report on magnetic hyperthermia.[33] Our results suggest that the optimum strength of the applied magnetic field that yields an increase in temperature without inducing any Foucault's currents is ~40 mT.

**Toxicity of the Ch-Std Incubated with MDA-MB-231 Cells and Exposed (or not) to an AMF.** In order to determine the optimum conditions for the therapy to work,[34] the percentage of living MDA-MB-231 cells, *i.e.*, the cells that are not in apoptosis, was estimated as a function of the strength of the applied magnetic field, of the quantity of Ch-Std incubated, of the incubation time, and of the number of heating cycles. For that, the cells were seeded on the same Petri dishes as in the previous section and grew during 24 h. After this initial period of growth, the cells were incubated in the presence (or not for the control) of the various types of nanoparticles during 24 h (D1), 48 h (D2), or 72 h (D3). At the end of the incubation time, the cells were exposed (or not for the control) to an AMF of frequency 183 kHz and strengths 20, 40, or 60 mT. The treatment was carried out during 20 min either one time or two times. Following the treatment, the cells were washed and harvested, and the percentage of living cells remaining was estimated using a flow cytometer. Provided the concentration of Ch-Std incubated with the cells remains below a certain threshold (0.5 mg/mL), the percentage of living cells is close to 100% (Figure 2d–f). For a concentration of Ch-Std incubated of more than 0.5 mg/mL, the percentage of living cells decreases below 60% (Figure 2d–f).

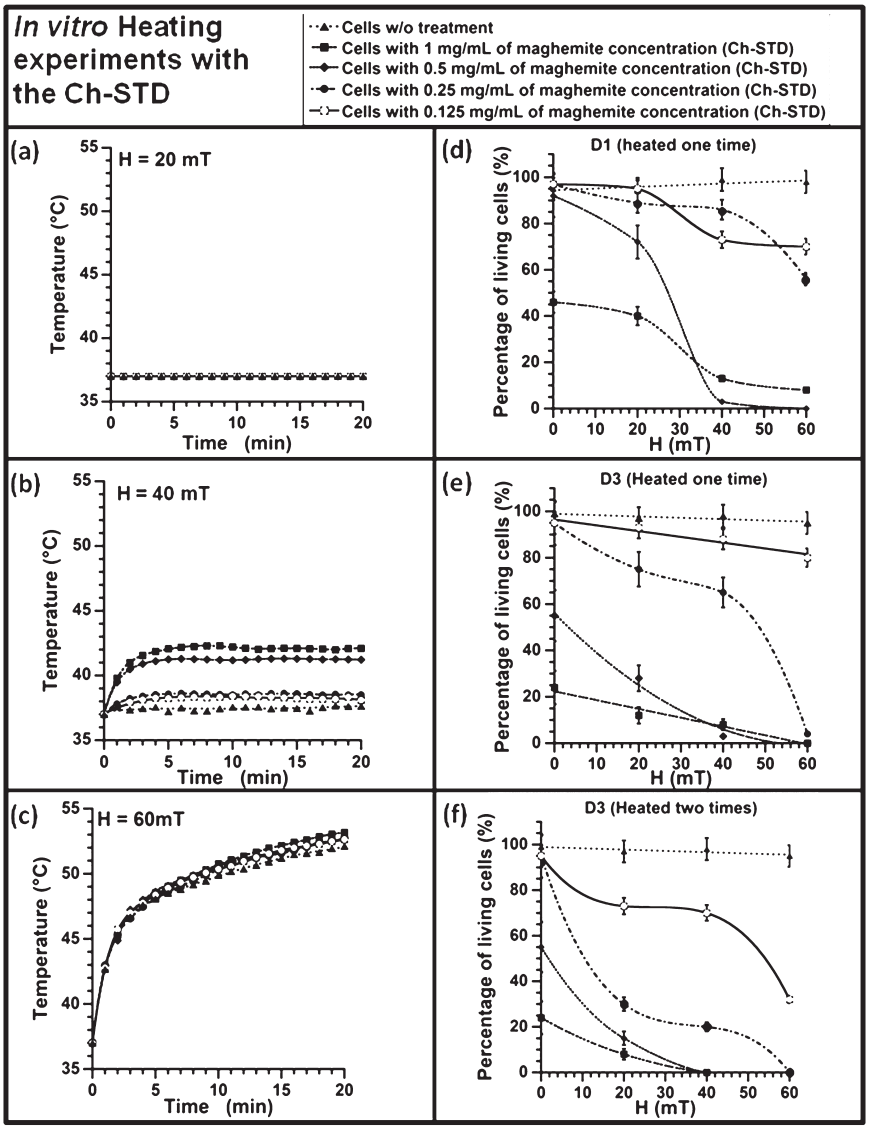


**Figure 2. Properties of suspended MDA-MB-231 cells incubated in the absence or in the presence of extracted chains of magnetosomes of various concentrations (0.125 mg/mL < $C_{\gamma Fe203}$ < 1 mg/mL, where $C_{\gamma Fe203}$ represents the concentration in maghemite of the suspensions) and exposed to an alternative magnetic field of frequency 183 kHz and various strengths (0 mT < *H* < 60 mT, where *H* represents the strength of the applied magnetic field). (a–c) Variations of temperature of suspensions containing MDA-MB-231 cells incubated in the absence or in the presence of chains of magnetosomes of various concentrations (0.125 mg/mL< $C_{\gamma Fe203}$ < 1 mg/mL) when an alternative magnetic field of strength *H* = 20 mT (a), *H* = 40 mT (b), or *H* = 60 mT (c) is applied to these suspensions. (d–f) Percentage of living adherent MDA-MB-231 cells as a function of the strength of the applied AMF (0 mT < *H* < 60 mT), which was applied once or twice during 20 min. The cells are either incubated during 24 h, D1 (d) or 72 h, D3 (e, f) either in the absence or in the presence of the extracted chains of magnetosomes of various concentrations as indicated.**

In the latter conditions, the percentage of Ch-Std internalized within the cells may be significant, which could explain the toxicity induced by their presence. Micrograph observations of MDA-MB-231 cells incubated during 24 h in the presence of 1 mg of Ch-Std have indeed revealed the presence of iron within the cells (Suppl. Figure 1), suggesting that the Ch-Std have penetrated within the cells at this high concentration. When the suspension containing only the MDA-MB-231 cells (without the Ch-Std) was exposed to an AMF of strength ~20, ~ 40, or ~60 mT, the percentage of living cells remained high, *i.e.*, close to 100%, as shown in Figure 2d–f, indicating that the AMF is not toxic in these conditions. By contrast, when the cells were incubated in the presence of the Ch-Std and exposed to the AMF, Figure 2d–f show the partial or total destruction of the cells, where the percentage of cell destruction increases with increasing magnetic field strength, incubation time, quantity of Ch-Std incubated, and number of heating cycles. For a magnetic field of 40 mT, determined as the optimum magnetic field strength in the previous section, up to 80% of the cells were destroyed for a concentration of Ch-Std incubated of 0.25 mg/mL, an incubation time of 72 h, and two heating cycles (Figure 2f).

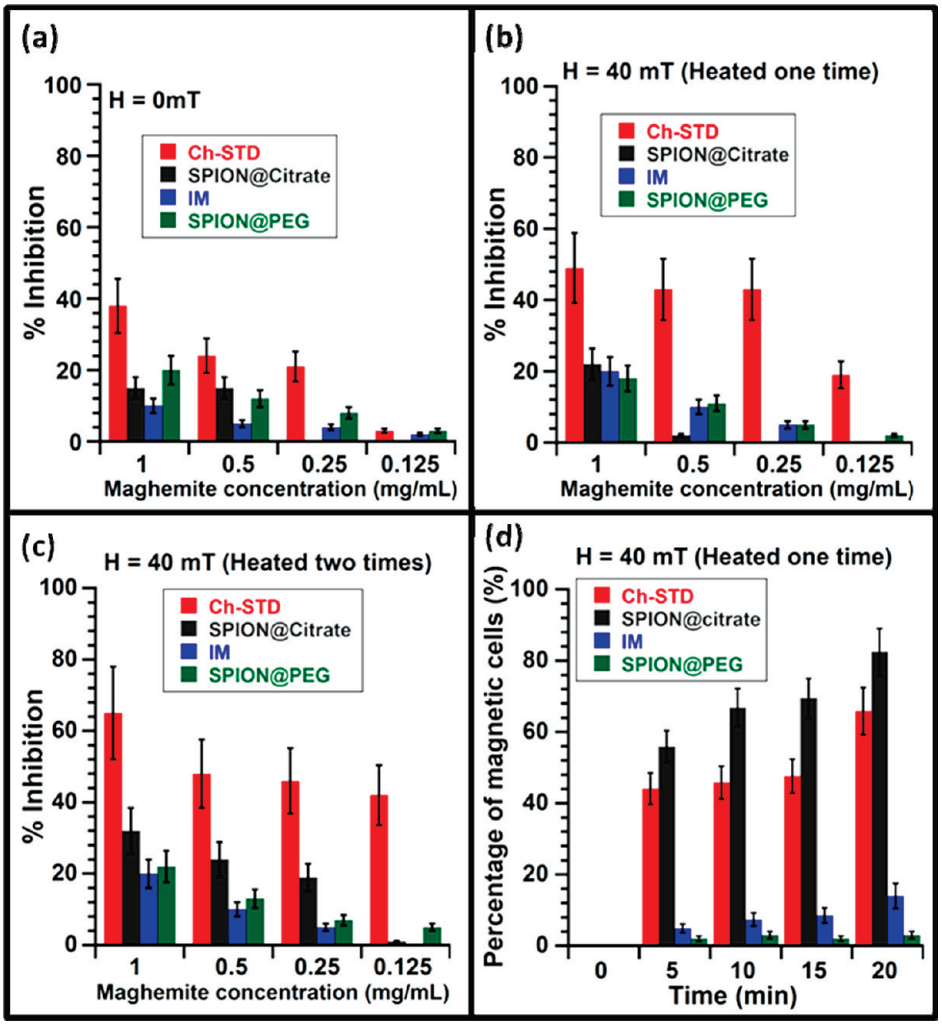


**Figure 3. (a–c) Percentage of inhibition of MDA-MB-231 cells incubated in the presence of four different suspensions containing either chains of magnetosomes (Ch-Std), individual magnetosomes (IM), SPION covered by citrate ions (SPION@Citrate), or SPION covered by PEG molecules (SPION@PEG) as a function of the concentration in maghemite of these four suspensions. The cells were either not exposed to an AMF (a), exposed once to the AMF of strength 40 mT (b), or exposed twice to the AMF of strength 40 mT (c). (d) Percentage of cells that become magnetic as a function of the incubation time when the four suspensions mentioned above (0.125 mg/mL < $C_{\gamma Fe_2O_3}$ < 1 mg/mL) are incubated in the presence of MDA-MB-231 cells and exposed to an AMF of frequency 183 kHz and strength of 40 mT.**

***In Vitro* Antitumoral Activity of the Ch-Std Compared with That of the IM, SPION@Citrate, and SPION@PEG.** The percentage of inhibition of MDA-MB-231 cells, *i.e.*, the percentage of these cells that stop growing in the presence of the Ch-Std, IM, SPION@Citrate, SPION@PEG, and/or AMF, was estimated using the microculture tetrazolium (MTT) assay. For that, the cells were seeded at a density of $2 \times 10^4$ cells per well in 96-well flat bottom plates and incubated within the culture medium during 24 h at 37 °C in an atmosphere containing 5% $CO_2$. Then the culture medium was removed and replaced by a 10% fetal calf serum (FCS) medium containing the various nanoparticles at different concentrations. These suspensions were then exposed (or not for the control) to an AMF of frequency 183 kHz and strength 40 mT, and the treatment was carried out during 20 min either one time or two times. After 72 h of incubation, the cells were washed with a phosphate-buffered saline (PBS) and incubated with 0.1 mL of MTT (2 mg/mL) for an additional 4 h at 37 °C. The insoluble product (composed essentially of formazan) was then dissolved by adding 100 $\mu$L of DMSO (Sigma). The absorbance of solubilized formazan was measured at 570 nm using a Labsustem Multiscan MS absorbance microplate reader. It provided an estimate of the number of functional mitochondria, a number that is proportional to the number of living cells. The percentage of inhibition was then estimated as the number of dead cells, *i.e.*, the cells in apoptosis, divided by the total number of cells.

Figure 3a–c show the percentage of inhibition of these cells incubated in the presence of the various types of nanoparticles not exposed to an AMF (Figure 3a), exposed to an AMF of 40 mT during 20 min (Figure 3b), or exposed to an AMF of 40 mT twice during 20 min (Figure 3c). Figure 3a shows that for 1 mg of Ch-Std incubated with the cells, the percentage of inhibition

is 38% in the absence of the AMF. Such a high percentage of inhibition could be explained by the internalization of the Ch-std within the cells (Suppl. Figure 1), which would prevent the cells from dividing. For lower concentrations of Ch-Std incubated the percentage of inhibition decreases significantly down to 3% for 0.125 mg/mL of Ch-Std incubated (Figure 3a). This indicates that in the absence of the AMF, the percentage of inhibition remains low provided the concentration of Ch-Std remains below a threshold of 0.125 mg/mL. In all conditions tested, the percentage of inhibitions of the cells is larger for the MDA-MB-231 cells incubated in the presence of the Ch-Std than for those incubated in the presence of all other types of nanoparticles tested (IM, SPION@Citrate, and SPION@PEG). The higher efficiency of the Ch-Std compared with that of the SPION@citrate or SPION@PEG could be explained by the higher SAR of the magnetosomes.[19] The higher efficiency of the Ch-Std for a given mass of material mainly arises from the difference in sizes between the magnetosomes of mean size 45 nm, which possess a ferromagnetic behavior at physiological temperature, and the SPION of sizes below 20 nm, which are superparamagnetic at this temperature. Chemically synthesized nanoparticles could potentially have the same SAR as the magnetosomes if they were monodomain, well-crystallized nanoparticles of the same sizes and composition as the magnetosomes. However, abiotic nanoparticles have not yet reached the heating efficiency of the magnetosomes, probably because of the difficulty to chemically synthesize monodomain, well-crystallized ferromagnetic nanoparticles with good stability. The higher heating capacity of the magnetosomes compared with that of SPION could be a real advantage when the nanoparticles are administered intravenously. In this case, a high percentage of nanoparticles may indeed be lost before the nanoparticles reach the tumor. If a small amount of nanoparticles is located within the tumor, the magnetosomes are more likely to release a sufficient amount of heat and yield antitumoral activity than the SPION due to their higher SAR. Since the Ch-Std and IM are both made of magnetosomes, the difference in efficiency between these two types of magnetosome arrangements cannot arise from a difference in SAR between them. Instead, we examine if this behavior is due to a different ability of cell magnetization in the presence of the IM than in that of the Ch-Std. To measure the percentage of magnetic cells, the cells were collected following treatment by positioning a strong magnet of 0.6 T close to the cell suspension. The supernate containing the cells that were not attracted by the magnet was removed, while the cells that had been attracted by the magnet were resuspended in 1 mL of PBS. The percentage of the cells attracted by the magnet, designated as magnetic cells, was then estimated using a flow cytometer. Figure 3d shows the percentage of MDA-MD-231 cells that become magnetic when the cells are incubated in the presence of the various types of nanoparticles and exposed (or not) to an AMF of ~40 mT applied during 5 to 20 min. The percentage of magnetic cells is high for the cells incubated in the presence of the Ch-Std (50−70%, Figure 3d), while it is very low for the cells incubated in the presence of the IM (less than 10%, Figure 3d). This difference in behavior between the Ch-Std and the IM may be due to a different type of organization between the Ch-Std, which are homogeneously distributed, and the IM, which are prone to aggregation. The mechanism of cell magnetization in the presence of the Ch-Std exposed to the AMF could be due to the Ch-Std that either penetrate within the cells or bind at the cell membranes.[35] This behavior could arise from the forces applied by the AMF on the Ch-Std or from a temperature increase, which would make the cell membrane permeable. We conclude from these results that the high efficiency of the Ch-Std is due on one hand to the high SAR of the magnetosomes and on the other hand to their ability to magnetize the cells in the presence of the AMF.

**TABLE 1. Conditions of Treatment of the Different Groups of Mice**

| group | mouse | AMF | suspension administered containing | quantity of iron oxide (mg) |
|---|---|---|---|---|
| 1 | 1, 2, 3, 4 | yes | Ch-Std | 1 |
| 2 | 5, 6, 7, 8 | yes | Ch-EDTA | 1 |
| 3 | 9, 10, 11, 12 | yes | SPION@Citrate | 1 |
| 4 | 13, 14, 15, 16 | yes | SPION@PEG | 1 |
| 5 | 17, 18, 19, 20 | yes | IM | 2 |
| 6 | 21, 22 | yes | linactive magnetotactic bacteria | 2 |
| 7 | 23, 24, 25 | no | Ch-Std | 1 |
| 8 | 26, 27, 28 | no | Ch-EDTA | 1 |
| 9 | 29, 30, 31 | no | SPION@Citrate | 1 |
| 10 | 32, 33, 34 | no | SPION@PEG | 1 |
| 11 | 35, 36, 37 | no | IM | 2 |
| 12 | 38, 39 | no | inactive magnetotactic bacteria | 2 |

**Antitumoral Activity and Heating Efficiency of the Ch-Std and Ch-EDTA Evaluated *in Vivo*.** Xenografted breast tumors were grown subcutaneously on both the right and left flanks of 39 mice. In one group of mice (group 1, Table 1), 100 $\mu$L of a suspension containing 10 mg/mL of Ch-Std was administered within the right tumors, while PBS was injected within the left tumors. These mice were exposed to an AMF of strength 40 mT and frequency 183 kHz during 20 min. The treatment was repeated three times with a one-day resting time separating each heating cycle. In another group of mice (group 7, Table 1), 100 $\mu$L of a suspension containing 10 mg/mL of Ch-Std was administered within their right tumor without further exposure to the AMF. When the mice of group 1 were exposed to the AMF, the temperature measured at the location of the Ch-Std injection increased by 10 °C from 33 to 43 °C within 20 min (Figure 4a). These temperatures lie within the range of temperatures reached during a typical hyperthermia treatment.[2] From the

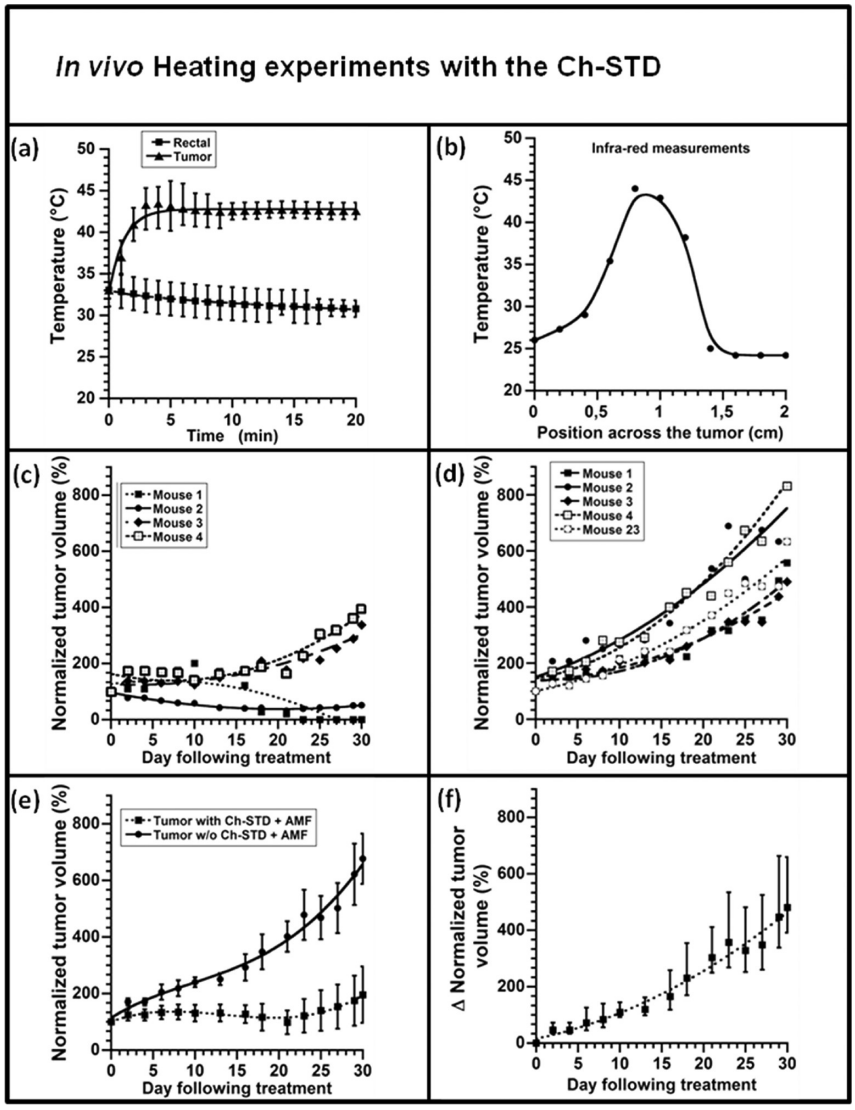


**Figure 4. Study of the mice treated with suspensions containing Ch-Std (groups 1 and 7). (a) Variations of the tumor and rectal temperatures when the AMF is applied during the treatment (group 1). The temperature is averaged over the different mice (mice 1 to 4). (b) For a mouse showing a typical behavior, temperature distribution measured across the treated tumor 10 min after the beginning of the treatment. (c) Evolution of the normalized tumor volume for the tumor in which the suspension containing the Ch-Std has been injected. The volume of the treated tumor is normalized by the volume of the tumor at the time of the treatment. (d) Same as in (c) for the control tumor in which only PBS has been injected. In mouse 23 (group 7), the suspension containing the Ch-Std has been injected, but the mouse has not been exposed to the AMF. (e) Average normalized tumor volume of a tumor having received Ch-Std and exposed to the AMF and of the tumor not having received the Ch-Std and exposed to the AMF. The averages are the means of the normalized tumor volumes over the different mice treated (mice 1 to 4). The error bars reflect the differences observed between the measurements carried out on the different mice. (f) Difference between the averaged normalized volumes of the treated and untreated tumors shown in (e).**

initial slope of the variation of temperature with time shown in Figure 4a, $\delta T/\delta t$ = 0.07 °C/s, we deduced a value of the SAR of ~380 W/$g_{Fe}$, using the relation SAR = $C_{water}(\delta T/\delta t)1/x_m$, where $C_{water}$ = 4.2 J/g·K is the specific heat of water and $x_m$ is the concentration of iron in grams per milliliters of water.[19] This value of the SAR is similar to that of ~390 W/$g_{Fe}$ measured previously for the Ch-Std mixed homogenously in an agarose gel and exposed to the same AMF (Table 2).[19] This suggests that the Ch-Std heat the tumor homogenously, a result that is further confirmed by the infrared measurements carried out during the heating cycle (Figure 4b). Indeed, these infrared measurements show a large spread of temperatures higher than 37 °C at the skin surface of the tumor. Figure 4b shows that the full width at half-maximum of the spatial temperature distribution is 0.75 cm, a value close to the lateral size of a tumor (~1 cm). Figure 4c and d show the normalized tumor volume, *i.e.*, the tumor volume measured 2 to 30 days following the treatment divided by the tumor volume measured during the day of the treatment, for the mice belonging to groups 1 and 7 (Table 1). During the 30 days following the treatment, the normalized volume of the right tumors of the mice belonging to group 1

decreased in three mice and the tumor completely disappeared in one mouse (Figure 4c). By contrast, the normalized volume of the left tumors of these mice and those belonging to group 7 strongly increased during the same period of time (Figure 4d). The normalized tumor volumes averaged over the different mice treated increased much less for the right than for the left tumors, as shown in Figure 4e. Moreover, the difference between the normalized tumor volumes of the right and left tumors strongly increased during the days following the treatment (Figure 4f), indicating the efficiency of the treatment with the Ch-Std. The progressive disappearance of the tumor treated by administering the Ch-Std within the tumor and by exposing the mice to the AMF can be observed in one of the mice (mouse 1) by examining the set of three photographs presented in Figure 5a, which were taken either during the day of the treatment (D0), 14 days after the treatment (D14), or 30 days after the treatment (D30). Thirty days following the treatment, Figure 5a shows a black spot at the position where the tumor had initially grown. The antitumoral activity was further revealed by histological examinations, which showed that there

**TABLE 2. Specific Absorption Rate of the Different Suspensions Either Administered in the Tumor of the Mouse or Mixed in a Gel and Exposed to an AMF of Strength 40 mT and Frequency 183 kHz**

| | SAR ($W/g_{Fe}$) in the gel | SAR ($W/g_{Fe}$) in the tumor |
|---|---|---|
| Ch-Std | 390 | 380 |
| Ch-EDTA | N.A. | 875 |
| IM | 355 | 160 |
| whole inactive bacteria | 125 | N.A. |
| SPION@Citrate | N.A. | 230 |
| SPION@PEG | N.A. | 0 |

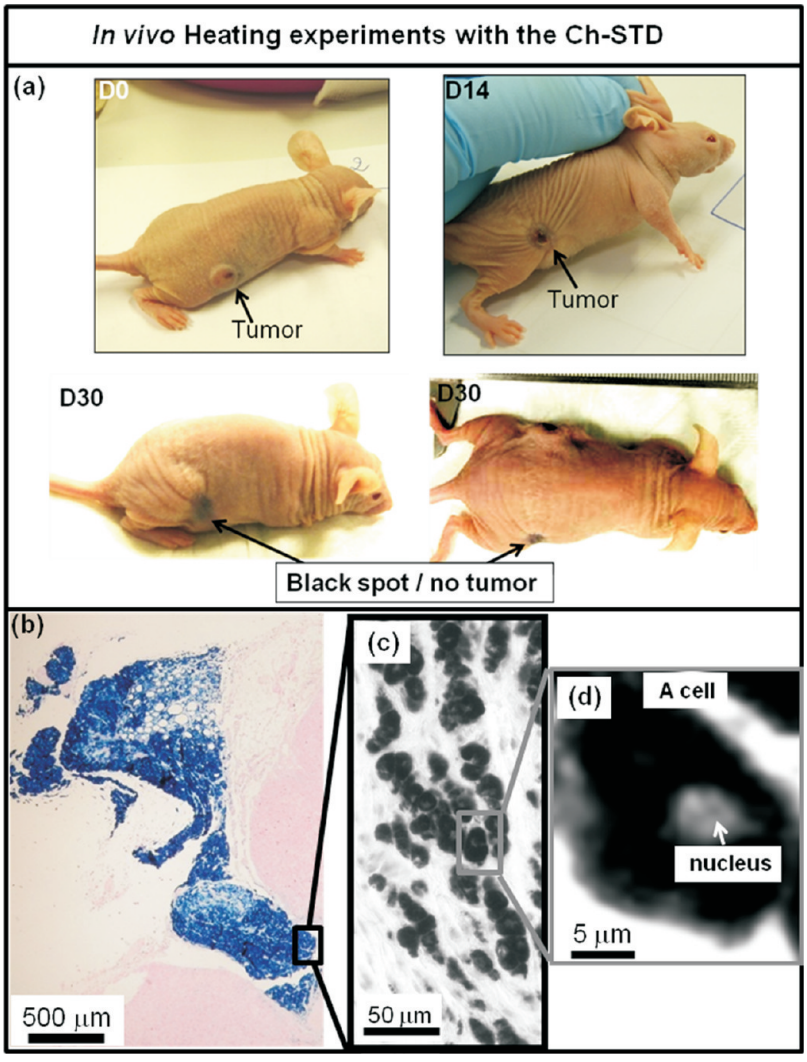


**Figure 5. Study of the mice treated with suspensions of chains of magnetosomes (group 1). (a) Photographs of the treated tumor in mouse 1 just after the treatment (D0), 14 days after the treatment (D14), 30 days after the treatment (D30). (b) Optical micrograph of a tumor tissue collected 30 days after the treatment in mouse 1 showing the presence of the bacterial magnetosomes (blue color or dark contrast). (c) Optical micrograph that is an enlargement of (b). (d) Optical micrograph that is an enlargement of (c) showing a cell with its nucleus surrounded by bacterial magnetosomes.**

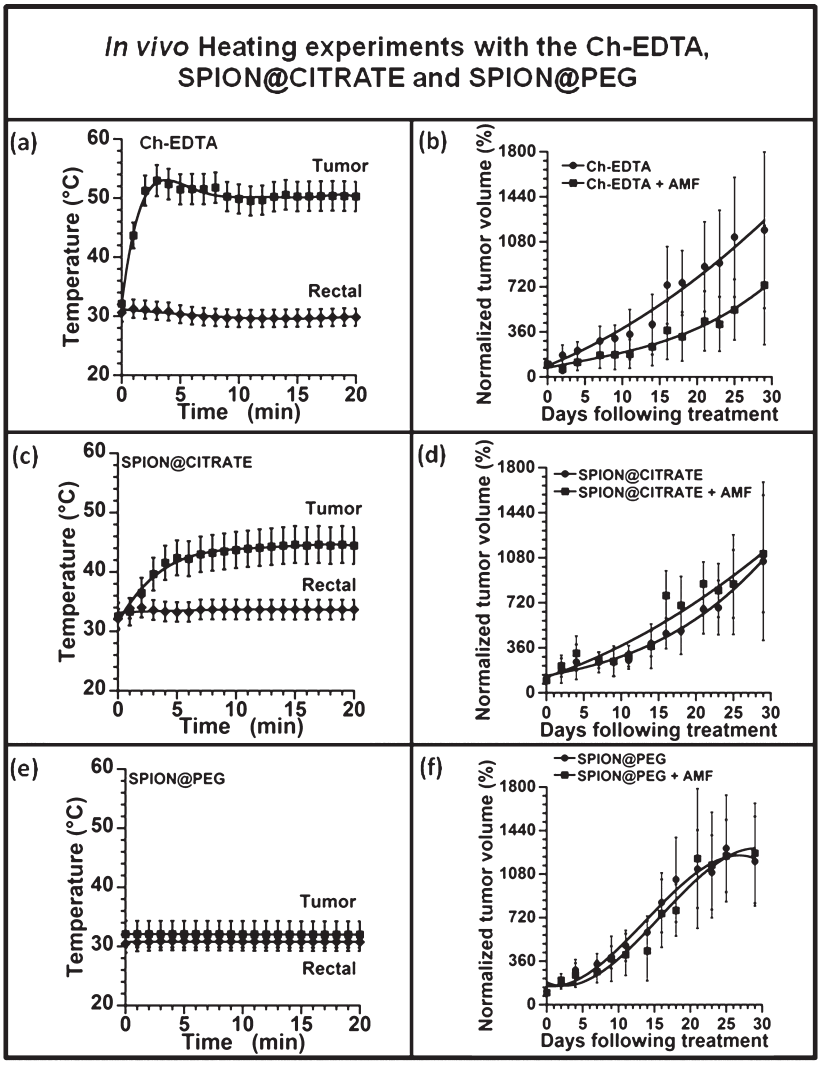


**Figure 6. (a, c, e) Variations of the tumor and rectal temperatures when the suspensions containing the Ch-EDTA, group 2, (a), the SPION@Citrate, group 3, (c), or the SPION@PEG, group 4, (e) are administered within the tumor and the alternative magnetic field of frequency 183 kHz and strength 40 mT is applied during 20 min. The treatment is repeated 3 times with a 1 day resting time between the different treatments. (b, d, f) Variations of the normalized tumor volume (*i.e.*, the tumor volume measured at day 2 to day 30 following the treatment divided by the tumor volume measured during the day of the treatment) during the days following the treatment for the treatment with the Ch-EDTA, groups 2 and 8, (b), the SPION@Citrate, groups 3 and 9, (d), or the SPION@PEG, groups 4 and 10, (f). In (b), (d), and (f), the error bars are the standard deviations estimated by taking into account the difference in normalized tumor volume between each mouse.**

was no sign of tumor tissues in mouse 1 (data not shown). Examinations of the treated tumors showed that the number of observed mitoses was low (4 on average by selected field of 300 $\mu m^2$), indicating a decrease in the activity of tumor proliferation. In mouse 23 and in two other mice where the suspension containing Ch-Std was injected without application of the alternative magnetic field, the tumor size increased strongly during the 30 days following the treatment, as shown in Figure 4d. This indicates that the antitumoral activity is due to the heat released by the Ch-Std and not solely to the presence of the Ch-Std within the tumor. To further understand the origin of the antitumoral activity of the Ch-Std, a micrograph of a tumor tissue collected after the treatment is presented in Figure 5b. It shows a homogeneous distribution of iron indicated by the large blue spread, suggesting a homogeneous distribution of the Ch-Std. This behavior could explain the homogeneous temperature distribution observed by infrared measurements. The enlargements of Figure 5b, which are shown in Figure 5c and d, show a black region surrounding the cell nucleus, suggesting that the chains of magnetosomes have penetrated within the cells after application of the alternative magnetic field, a behavior that could explain the cell magnetization (Figure 3d) and suggests a mechanism of intracellular heating. The impact of the length of the magnetosome chains on the efficiency of the thermotherapy was further examined by administering within the tumors Ch-EDTA, which are longer chains of magnetosomes than the Ch-Std. After administration of 100 $\mu$L of a suspension containing 10 mg/mL of Ch-EDTA within the right

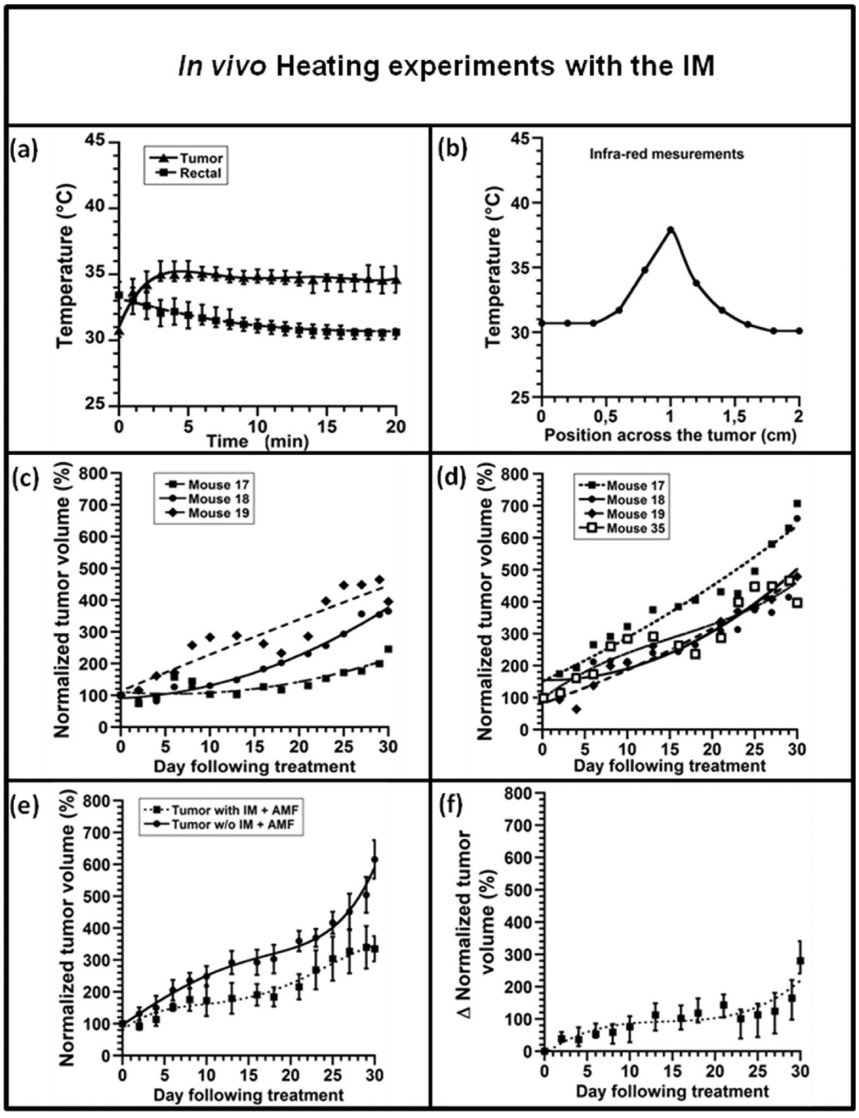


**Figure 7. Study of mice treated with suspensions of individual magnetosomes (groups 5 and 11). (a) Variations of the tumor and rectal temperatures when the magnetic field is applied during the treatment. These temperatures are averaged over the different mice treated (mice 17 to 19). (b) For a mouse showing a typical behavior, the temperature distribution measured across the treated tumor 10 min after the treatment has started. (c) Variation of the normalized tumor volume for the tumor in which the suspension of individual magnetosomes has been injected (mice 17 to 19). The volumes of the tumors are normalized by the volume of the tumor at the time of the treatment. (d) Same as in (c) for the so-called control tumor, in which only PBS has been injected. In mouse 35, the suspension of individual magnetosomes has been injected, but no magnetic field has been applied. (e) Average normalized tumor volume for a tumor having received the IM and exposed to the AMF and for the tumor not having received the IM and exposed to the AMF. The averages are the means of the normalized tumor volumes measured over the different mice treated. The error bars reflect the difference between the measurements of the different mice. (f) Difference between the averaged normalized volumes of the treated and untreated tumors shown in (e).**

tumors of the mice belonging to group 2 followed by the application of the AMF, the tumor temperature increaseed more rapidly with the Ch-EDTA than with the Ch-Std, as revealed by comparing Figure 6a with Figure 4a. As with the Ch-Std, it is possible to completely eliminate the tumor with the Ch-EDTA. However, as a whole, the antitumoral activity is less pronounced with the Ch-EDTA than with the Ch-Std. While the size evolutions of the right and left tumors averaged over the different mice studied were significantly different for the treatment with the Ch-Std (Figure 4c and d), they were relatively similar for the treatment with the Ch-EDTA (Figure 6b). It is possible that the Ch-EDTA penetrate less easily than the Ch-Std within the cancer cells due to their longer length, hence reducing the amount of intracellular heating that they can produce. We deduce from these results that the efficiency of the thermotherapy may be determined not only by the amount of heat produced by the chains of magnetosomes but also by the length of the chains of magnetosomes.

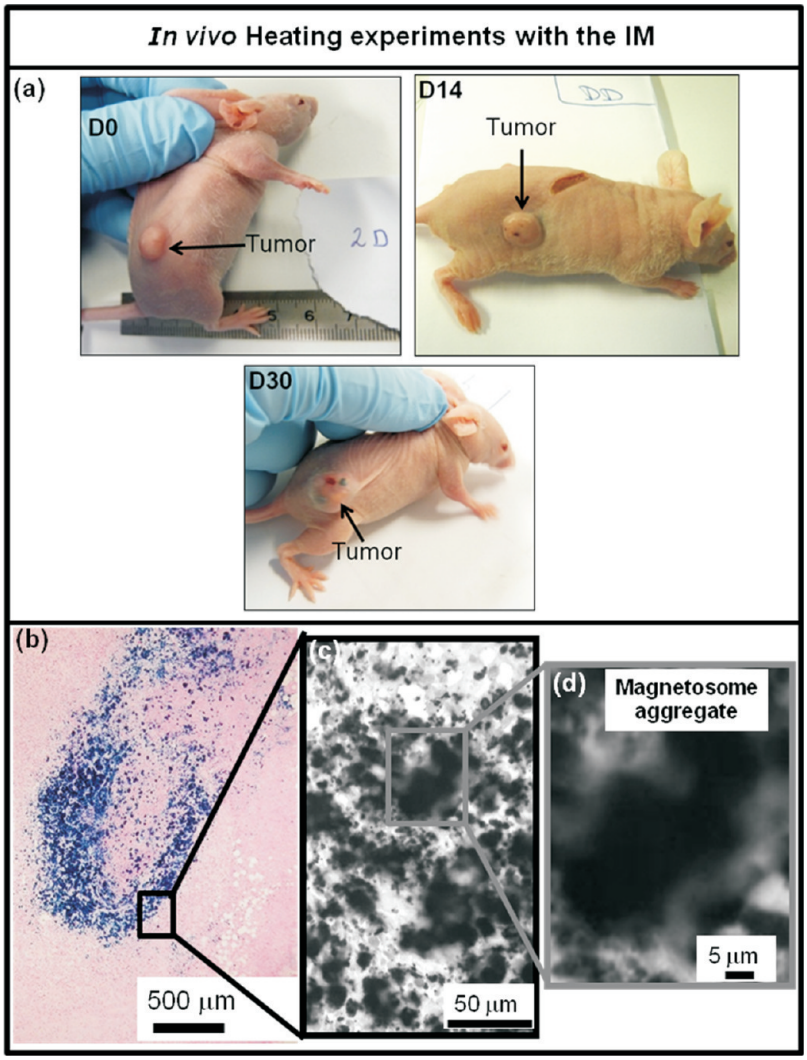


**Figure 8. Study of a typical mouse treated with individual magnetosomes (mouse 17). (a) Photographs of the treated tumor in mouse 17 just after the treatment (D0), 14 days after the treatment (D14), or 30 days after the treatment (D30). (b) Optical micrograph of a tumor tissue collected 30 days after the treatment in mouse 17. (c) Optical micrograph that is an enlargement of a region in (b) showing the presence of bacterial magnetosomes (blue color or dark contrast). (d) Optical micrograph that is an enlargement of a region in (c) showing magnetosome aggregates and the absence of the cell nucleus.**

**Lower Heating Efficiency and Antitumoral Activity of the SPION@Citrate, SPION@PEG, IM, and Whole Inactive Magnetotactic Bacteria Compared with Those of the Ch-Std and Ch-EDTA.** Following the same method as that used with the Ch-Std and Ch-EDTA, the mice received intratumoraly within their right tumor 100 $\mu$L of five different suspensions containing either ~1 mg of SPION@Citrate (group 3, Table 1), ~1 mg of SPION@PEG (group 4, Table 1), ~2 mg of IM (group 5, Table 1), or $10^8$ magnetotactic bacteria (group 6, Table 1). The suspension containing the IM was chosen as twice that of the Ch-Std to yield similar heating properties in solution between the IM and the Ch-Std. The left tumors were used as internal control and received only PBS. These mice were then exposed to an AMF of strength 40 mT and frequency 183 kHz, which was applied during 20 min. The treatment was repeated three times with a one-day resting time separating each heating cycle. The mice belonging to groups 7 to 12 were treated the same as those belonging to groups 2 to 6 except that they were not exposed to an AMF (Table 1). When 1 mg of SPION@Citrate was administered within the right tumor of the mice belonging to group 3 and the mice were exposed to the AMF, Figure 6c shows that the tumor temperature increased by a low amount of 4 °C in 2 min. Most probably due to this small temperature increase, the thermotherapy was inefficient. The volume of these tumors increased at the same rate as those of the tumors used as internal control during the 30 days following the treatment, as shown in Figure 6d. Moreover, none of the mice showed a complete disappearance of the tumor during the 30 days following the treatment. Following the administration of the SPION@PEG within the right tumors of the mice belonging to group 4 and application of the

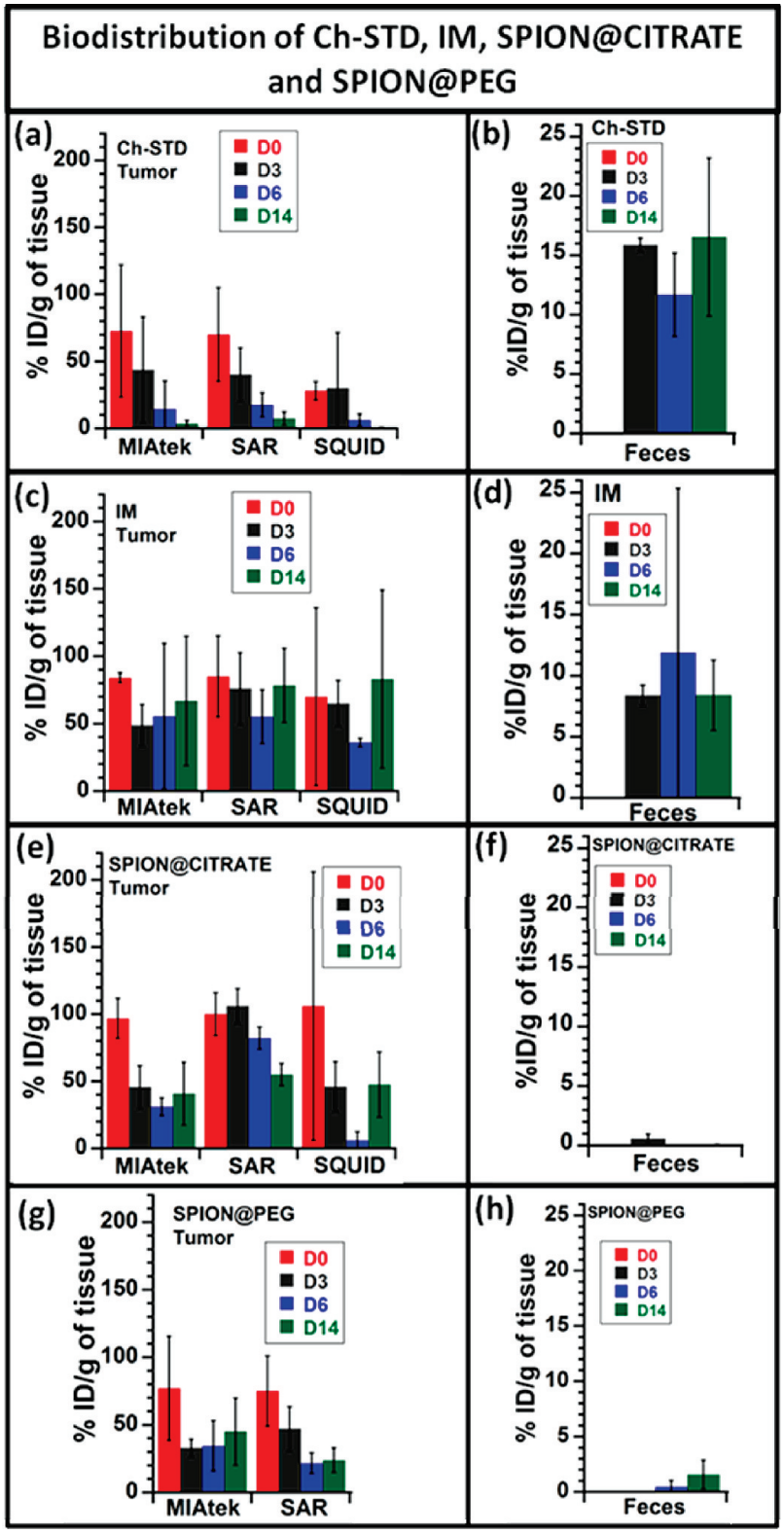


**Figure 9. Percentage of nanoparticules in the tumor (a, c, e, g) and in the feces (b, d, f, h) at the time of the injection (D0), 3 days after the injection (D3), 6 days after the injection (D6), and 14 days after the injection (D14) for an intratumoral administration of suspensions containing either Ch-Std (a, b), IM (c, d), SPION@Citrate (e, f), or SPION@PEG (g, h).**

same AMF as above, there was no increase of the tumor temperature, as shown in Figure 6e, and none of the tumors decreased in size during the 30 days following the treatment (Figure 6f). These results indicate the lower efficiency of the SPION@Citrate and SPION@PEG compared with that of the Ch-Std and Ch-EDTA.[36] Another

group of mice (group 5) was treated with the individual magnetosomes, which possess the same SAR and composition in iron oxide as the magnetosomes organized in chains but form individual nanoparticles. After application of the AMF, the tumor temperature of the mice treated with the IM increased by 4 °C from 31 to 35 °C (Figure 7a), which is a much smaller temperature increase than that observed with the Ch-Std or Ch-EDTA. Using the same method as for the Ch-Std and given that the initial slope of the variation of temperature with time of the heated IM is $\delta T/\delta t \approx 0.03$ °C/s (Figure 7a), a SAR of ~160 W/$g_{Fe}$ is estimated for the heated IM. This value is smaller than the SAR of ~355 W/$g_{Fe}$ deduced for the IM mixed homogeneously within a gel and heated under the same AMF (Table 2).[19] We deduce that, in contrast to the Ch-Std, the IM do not heat the tumor homogenously. This result is further confirmed by infrared measurements. After 10 min of heating, infrared measurements showed that the temperature spread within the tumor was ~0.5 cm (Figure 7b), which is less than that obtained with the Ch-Std. The less homogeneous temperature distribution of the IM compared with the Ch-Std could be explained by the fact that under the application of the AMF the IM remain aggregated outside of the cells, whereas a portion of the Ch-Std either penetrate within the cells or bind at the cell membrane while another portion of the Ch-Std remains outside of the cells. Figure 7c and d show that the normalized tumor volumes (as defined previously) of the heated and unheated tumors both increased during the 30 days following the treatment, indicating the lower antitumoral activity of the IM compared with that of the Ch-Std. The tumor volume averaged over the different mice treated increased less for the tumor treated with the IM than for the untreated tumor (Figure 7e). However, the difference between the volume of the untreated and treated tumor is much less pronounced with the IM than with the Ch-Std, as concluded by comparing Figures 4f and 7f. The increase of the treated tumor size can also be observed in a mouse showing a typical behavior (mouse 17) by examining the set of three photographs taken on the day of the treatment (D0), 14 days after the treatment (D14), and 30 days after the treatment (D30) (Figure 8a). Together these results indicate that neither the presence of the IM nor the heat that they generate in the presence of an AMF produces antitumoral activity, although the amount of magnetosomes injected is twice that contained in the suspension of Ch-Std or Ch-EDTA. Examinations of the tumor localized on the right flank of mouse 18 provided some explanation for this behavior. They show an important mass of necrotic cells in tumors collected 30 days after the first treatment, but mitoses are numerous and indicate an important tumor proliferative activity with an average of 12 mitoses per selected field of 300 $\mu m^2$ in size (data not shown). The Berlin blue staining of a pathological section obtained from the right tumor shows the presence of diffused dark spots (Figure 8b). These spots are presumed to arise from magnetosome aggregates, as shown in enlarged views of Figure 8b presented in Figure 8c and d. The presence of these aggregates prevents the magnetosomes from penetrating within the cells both in the absence and in the presence of the AMF (Figure 3d). With the IM, the absence of antitumoral activity could be explained in part by their relatively low *in vivo* heating efficiency and in part by their tendency to aggregate, which prevents them from distributing homogenously within the tumor and penetrating within the cancer cells. Finally, $10^8$ inactive magnetotactic bacteria containing 2 mg of iron oxide have also been administered within the tumors. After application of the AMF, the temperature increased by only 4 °C from 33 to 37 °C in 20 min. The density of chains of magnetosomes within the assembly of bacteria is probably too low to yield efficient heating. In this case, the absence of antitumoral activity was revealed by the increase in size of the treated tumors during the 30 days following the treatment and by histological examination, which revealed a pigmented area in the treated tumor with a high mitotic activity (15 mitoses on average in a selected field of 300 $\mu m^2$, data not shown). We conclude from these results that the magnetosomes need to be extracted from the magnetotactic bacteria in such a way that they preserve their original organization in chains to be used efficiently in thermotherapy.

**Biodistribution of the Ch-Std Compared with That of the IM, SPION@Citrate, and SPION@PEG.** Biodistribution studies have been carried out to study how long the various types of nanoparticles remain within the tumor after an intratumoral administration and to examine if they are well eliminated by the organism. For that, the various types of particles (Ch-Std, IM, SPION@Citrate, and SPION@PEG) were administered within the right tumors of 54 mice. The various suspensions were prepared at a concentration of 10 mg of maghemite per mL, and 100 $\mu$L of these suspensions was injected at a dose of 1 mg of maghemite. The amount of maghemite contained within the feces or the tumors of the mice was measured using either an instrument developed by our industrial partner Magnisense (the MIAtek), the magnetization of the various nanoparticles using a SQUID, or the SAR deduced from the heating curves of the heated tumors *ex vivo*, as described in more detail in the Materials and Methods section. These measurements were carried out during the day of the injection (day 0, D0), three days after the injection (day 3, D3), six days after the injection (day 6, D6), or 14 days after the injection (day 14, D14). On the different days (D0, D3, D6, and D14), the animals were euthanized by cervical dislocation and the tissues or organs of interest (blood, liver, spleen, lung, kidney, tumor, feces) were collected immediately, weighed, and frozen at 4 °C until analysis.

Figure 9a shows the biodistribution of the Ch-Std within the tumors (estimated as the percentage of injected dose per gram of tissue) just after the injection (D0), 3 days after the injection (D3), 6 days after the injection (D6), and 14 days after the injection (D14). The three types of measurements (MIAtek, SAR, and SQUID) show essentially the same trend: The rapid decrease of the percentage of Ch-Std contained within the tumors during the 14 days following their injection (Figure 9a). Indeed, more than 90% of the Ch-Std was eliminated within 14 days following the injection. The Ch-Std were found essentially in the feces with 10−15% in the feces at the first day postinjection (D1) (data not presented in Figure 9b) and 15−20% at day 3 (D3), day 6 (D6), and day 14 (D14) postinjection (Figure 9b). With the Ch-Std, the route of elimination appears to be essentially fecal. Only small traces of Ch-Std (<0.1% ID/g of tissue) were found in the lung, kidney, liver, and spleen the third day (D3) and the sixth day (D6) following the injection. No Ch-Std were found in the blood. These results suggest that the Ch-Std were rapidly excreted. Compared with the Ch-Std, Figure 9c shows that the percentage of IM contained within the tumor decreases less significantly during the 14 days following the treatment. A lower percentage of 5−10% of IM was found in the feces at D3, D6, and D14 (Figure 9d), suggesting a less rapid elimination of the IM compared with that of the Ch-Std. The SPION@Citrate and SPION@PEG also seem to be eliminated less easily than the Ch-Std. Figure 9e and g show that a large percentage of them remained within the tumors during the 14 days following their injection. In addition, almost no SPION@Citrate nor SPION@PEG were found in the feces (Figure 9f and h). This could be explained by the metabolization of these nanoparticles into free iron complexes, which would rather be a drawback of these chemically synthesized nanoparticles compared with the magnetosomes since free iron can cause oxidative stress.[37]

## CONCLUSIONS

The antitumoral activity of the chains of magnetosomes extracted from AMB-1 magnetotactic bacteria is essentially due to three factors: (i) the large amount of heat that they produce when they are exposed to an AMF, which essentially comes from the large sizes and ferromagnetic behavior of the magnetosomes; (ii) their faculty of magnetizing MDA-MB-231 breast cancer cells, enabling efficient heating and cell destruction; and (iii) the arrangement of the magnetosomes in chains, which favor a homogeneous temperature distribution within the tumor tissue. In the conditions that we tested, we could observe the complete disappearance of a tumor xenografted under the skin of a mouse by administering ∼1 mg of chains of magnetosomes directly within the tumor and by applying an AMF of frequency 183 kHz and strength 40 mT three times during 20 min. By contrast, no or much less efficient antitumoral activity was observed when the mice were treated with the same quantity (in mass of iron oxide) of superparamagnetic iron oxide nanoparticles coated by citrate ions or by PEG molecules, which are currently being tested for AMF cancer therapy. This study thus shows the potential of chains of magnetosomes extracted from whole magnetotactic bacteria for application in alternative magnetic field cancer therapy.

## MATERIALS AND METHODS

**Preparation of the Different Types of Nanoparticles Used As Heating Sources.** We used the following six different types of nano particles as heating sources:

(i) whole inactive magnetotactic bacteria;

(ii) chains of magnetosomes extracted from magnetotactic bacteria, which have been cultivated in the conditions recommended by the ATCC in the absence of EDTA, designated as Ch-Std;

(iii) chains of magnetosomes extracted from magnetotactic bacteria, which have been cultivated by introducing an iron chelate (EDTA) within the bacterial growth medium of the ATCC, designated as Ch-EDTA;

(iv) individual magnetosomes extracted from magnetotactic bacteria and detached from the chains by heat and SDS treatment, designated as IM;

(v) chemically synthesized superparamagnetic iron oxide nanoparticles coated with citrate ions, designated as SPION@Citrate;

(vi) commercially available chemically synthesized superparamagnetic iron oxide nanoparticles covered by PEG molecules, designated as SPION@PEG.

**Preparation of the Whole Inactive Magnetotactic Bacteria, Ch-Std, Ch-EDTA, and IM.** *Magnetospirillum magneticum* strain AMB-1 was purchased from the American Type Culture Collection (ATCC 700274). Cells were grown microanaerobically at room temperature (∼25 °C) in liquid culture in slightly modified revised MSGM medium (ATCC Medium 1653). In one liter, this growth medium contained 0.68 g of monobasic potassium phosphate, 0.85 g of sodium succinate, 0.57 g of sodium tartrate, 0.083 g of sodium acetate, 225 μL of 0.2% resazurin, 0.17 g of sodium nitrate, 0.04 g of L-ascorbic acid, 2 mL of a 10 mM iron quinate solution, 10 mL of Woolf's vitamins, and 5 mL of Woolf's minerals. The iron quinate solution was prepared by dissolving 0.19 g of quinic acid and 0.29 g of $FeCl_3 \cdot 6H_2O$ in 100 mL of distilled water. The solution of Woolf's minerals contained in 1 L of distilled water 0.5 g of nitrilotriacetic acid ($C_6H_9NO_6$), 1.5 g of magnesium sulfate HEPTA ($MgSO_4 \cdot 7H_2O$), 1 g of sodium chloride, 0.5 g of manganese sulfate ($MnSO_4 \cdot H_2O$), 100 mg of ferrous sulfate heptahydrate ($FeSO_4 \cdot 7H_2O$), 100 mg of cobalt nitrate ($Co(NO_3)_2 \cdot 7H_2O$), 100 mg of calcium chloride ($CaCl_2$), 100 mg of zinc sulfate heptahydrate ($ZnSO_4 \cdot 7H_2O$), 10 mg of hydrate copper sulfate ($CuSO_4 \cdot 5H_2O$), 10 mg of aluminum potassium sulfate dodecahydrate ($AlK(SO_4)_2 \cdot 12H_2O$), 10 mg of boric acid ($H_3BO_3$), 10 mg of sodium molybdate ($Na_2MoO_4 \cdot 2H_2O$), 2 mg of sodium selenite ($Na_2SeO_3$), 10 mg of sodium tungstate dihydrate ($Na_2WO_4 \cdot 2H_2O$), and 20 mg of nickel chloride ($NiCl_2 \cdot 6H_2O$). The solution of Woolf's vitamins was prepared by dissolving in 1 L of distilled water 2.2 mg of folic acid (vitamin B9), 10.2 mg of pyridoxine (vitamin B6), 5.2 mg of riboflavin (vitamin B2), 2.2 mg

of biotin (vitamin H or B7), 5.2 mg of thiamin (vitamin B1), 5.2 mg of nicotinic acid (vitamin B3 or PP), 5.2 mg of pantothenic acid (vitamin B5), 0.4 mg of vitamin B12, 5.2 mg of amino benzoic acid, 5.2 mg of thiotic acid, and 900 mg of potassium phosphate. The pH of the growth medium was adjusted to 6.85 using a 5 M sodium hydroxide solution. Stationary phase occurred when the medium became completely reduced, as indicated by a change in the coloration of the growth medium, from pink to colorless.

Four different types of samples were prepared from intact whole cells of *M. magneticum* containing either whole magnetotactic bacteria, chains of magnetosomes extracted from magnetotactic bacteria with different lengths (Ch-Std or Ch-EDTA), or individual magnetosomes detached from the chains by heat and SDS treatments (IM).[29,30] Cells were harvested at stationary phase by centrifugation at 8000 rpm for 15 min. The supernatant (spent growth medium) was discarded, and cells were resuspended in 3 mL of deionized water. The first sample contained whole inactive magnetotactic bacteria, as shown in the TEM micrograph of Figure 1a. To extract the chains of magnetosomes, 1 mL of the cell suspension was centrifuged and resuspended in 10 mM Tris·HCl buffer (pH 7.4) and then sonicated for 120 min at 30 W to lyse the cells, thus releasing the chains of magnetosomes. Sonication times of 60 and 180 min were also tested and enabled extracting the chains of magnetosomes from the bacteria. For a sonication time of less than 60 min, the magnetotactic bacteria were not all lysed, while for a sonication time of more than 180 min, aggregation began to be observed due to the presence of individual aggregated magnetosomes. After sonication, the suspension of chains of magnetosomes was magnetically separated by placing a strong magnet in neodymium (0.1−1 T) next to the tube where the magnetic material was collected as a pellet. The supernate containing cell debris and other organic material was removed. The magnetosome chains were washed 10 times with a 10 mM Tris·HCl buffer (pH 7.4) in this way and were finally resuspended in sterile deionized water. A typical assembly of chains of magnetosomes extracted from the whole bacteria (Ch-std) is shown in the TEM micrograph of Figure 1b. The surface charge of the chains of magnetosome was measured as a function of pH using dynamic light scattering measurements (NanoZetasizer, Malvern Instruments Ltd.). At physiological pH, Suppl. Figure 2a shows that the surface charge of the chains of magnetosomes is negative at −22 mV. The infrared measurements were carried out using a Nicolet 380 FT IR Thermo Electro. The infrared absorption spectrum of a suspension of chains of magnetosomes was also recorded and is presented in Suppl. Figure 2b. It showed peaks arising from the functional groups carboxylic acid, amine, amide, and phosphate (P−O), revealing the presence of both proteins and phospholipids within the suspension of chains of magnetosomes. This result suggests that both the membrane surrounding the magnetosomes and the filament binding the magnetosomes are present in this sample.[21] Two different types of chains of magnetosomes extracted from magnetotactic bacteria were prepared, which were obtained by cultivating the bacteria either in the conditions of the ATCC as described above or in the presence of an iron chelate (0.4 $\mu$M EDTA), which was added to the standard ATCC growth medium. The presence of EDTA within the bacterial growth medium led to longer chains of magnetosomes and magnetosomes of larger sizes with enhanced heating properties in solution as compared with the chains of magnetosomes prepared in the standard conditions (Suppl. Figure 3). Individual magnetosomes (*i.e.*, magnetosomes that are not organized in chains) were obtained by heating the suspension of magnetosome chains for 5 h at 90 °C in the presence of 1% sodium dodecyl sulfate in deionized water to remove most of the biological material surrounding the magnetosomes, *i.e.*, most of the magnetosome membrane surrounding the magnetosomes and the cytoskeleton responsible for the alignment of the magnetosomes in each chain.[21] Individual magnetosomes were washed as described for magnetosome chains and resuspended in deionized water. The TEM micrograph of Figure 1c shows a typical assembly of individual magnetosomes. The individual magnetosomes possess different properties from the chains of magnetosomes. They form an aggregated assembly of nanoparticles (Figure 1c). They possess a surface charge that strongly depends on their level of aggregation. When the individual magnetosomes are sonicated and dispersed in water, they possess a relatively similar surface charge to that of the chains of magnetosomes at pH 7. However, when they are aggregated, the individual magnetosomes possess a positive charge (10 mV at pH 7, Suppl. Figure 2a). The individual magnetosomes are surrounded by phospholipid acid (presence of P−O peak in the infrared absorption spectrum of Suppl. Figure 2b), but not by proteins (absence of amide in the infrared absorption spectrum of Suppl. Figure 2b), suggesting that the biomaterial that surrounds the magnetosomes has not been completely removed but has been sufficiently denatured to yield individual magnetosomes not organized in chains.

**Preparation and Characteristics of the SPION@Citrate and SPION@PEG.** The chemically synthesized nanoparticles (SPION@Citrate) were prepared following a protocol described previously.[38] To prepare noncoated $\gamma Fe_2O_3$ particles, a solution of base (dimethylamine) was first added to an aqueous micellar solution of ferrous dodecyl sulfate ($Fe(DS)_2$) and mixed. The final reactant concentrations were $1.3 \times 10^{-2}$ and $8.5 \times 10^{-1}$ mol $L^{-1}$ for $Fe(DS)_2$ and dimethylamine, respectively. The solution was then stirred vigorously during 2 h at 28.5 °C, and the resulting precipitate of uncoated nanocrystals was isolated from the supernatant by centrifugation. In the second step, the precipitate was washed with an acidic solution ($HNO_3$, $10^{-2}$ mol $L^{-1}$) until a solution of pH = 2 was reached. Sodium citrate dissolved in water ($[Na_3C_6O_7H_5]$ = $1.5 \times 10^{-2}$ mol $L^{-1}$) was used to coat the nanoparticles. The solution was sonicated during 2 h at 90 °C, and the addition of acetone induced nanocrystal precipitation. After washing with a large excess of acetone, the precipitate was dried in air. The nanocrystals coated with citrate ions were finally dispersed in water. The pH, which was initially ~2, was progressively increased up to 7.4 by adding a solution of sodium hydroxide, NaOH ($10^{-1}$ mol $L^{-1}$). The SPION@Citrate are composed of maghemite and possess a mean size of ~10 nm. A TEM micrograph of the SPION@Citrate is shown in Suppl. Figure 2c. The detailed properties of the SPION@PEG can be obtained from the company Micromod. The information sheet (product-No. 79-00-201) provided by Micromod indicates that the SPION@PEG are made of maghemite, possess a saturating magnetization of 34 emu/g, a size of ~20 nm, and a polydispersity of less than 20%, and that they are stable in aqueous buffer at pH > 4.

**Estimates of the Concentrations of the Different Suspensions.** The concentrations of the suspensions containing the Ch-Std, the IM, and the SPION@Citrate represent the quantity of maghemite contained in 1 mL of water. They were estimated in three different ways, either by measuring the absorbance of these suspensions at 480 nm, by weighing the amount of nanoparticles or magnetosomes after lyophilization, or by measuring the saturation magnetization of 20 $\mu$L of each suspension deposited on top of a substrate using SQUID magnetometer measurement.[29,30] These three different types of measurements yielded the same estimate of the concentration for the suspensions containing individual magnetosomes and SPION. For the suspension containing the chains of magnetosomes, the presence of biological material surrounding the bacterial magnetosomes and the arrangement of the magnetosomes in chains led to an overestimate of the maghemite concentration by absorbance and lyophilization. Therefore the concentration of this suspension was determined using SQUID measurements. For the SPION@PEG, the concentration was known from the manufacturer. For the treatment with the whole magnetotactic bacteria, the bacterial concentration injected was $10^8$ cells in 100 $\mu$L. For the *in vitro* experiments, the concentrations of the suspensions containing the Ch-Std, IM, SPION@Citrate, and SPION@PEG was varied between 0.125 and 1 mg/mL. For the *in vivo* experiments, the concentrations of the different suspensions administered were chosen as 20 mg/mL for the suspension containing the IM or whole magnetotactic bacteria and 10 mg/mL for the other suspensions.

**TEM Measurements.** The TEM measurements of the different nanoparticles, which were essentially used to deduce magnetosome sizes and the magnetosome chain lengths, were carried out following a method described elsewhere.[29,30]

***In Vitro* MTT Tests.** MDA-MB-231 cells were obtained from the American Type Culture Collection (ATCC). The cell lines were cultivated in Dulbecco's modified Eagle's medium supplement, which contained 10% fetal calf serum, 2 mM L-glutamine, 1 mM sodium pyruvate, and 50 U/mL streptomycin (all purchased from Life Technologies Inc.). Cell viability was evaluated using the so-called microculture tetrazolium assay.[39] This technique measures the ability of mitochondrial enzymes to reduce 3-(4,5-dimethylthiazol-2-yl)-2,5-diphenyltetrazolium bromide (purchased from Sigma, St Louis, MO, USA) to purple formazan crystals.

**Estimate of the Percentage of Living MDA-MB-231 Cells *in Vitro*.** The percentage of living cells was estimated *in vitro* to evaluate the efficiency of the thermotherapy. Following the incubation of the cells with the Ch-Std described in the main text, the cells were washed twice with PBS. In order to harvest the cells, 250 $\mu$L of Trypsin-EDTA was added to the adherent cells. Then 750 $\mu$L of the liquid medium was added to the harvested cells to homogenize the suspension. The suspension was then centrifugated at 700*g* during 3 min, the supernate was removed, and the cells were resuspended in 1 mL of PBS. In order to evaluate the percentage of living cells, 5 $\mu$L of propidium iodide (PI) (1 mg/mL mixed in ethanol, Sigma Aldrich) was added to the cell suspensions. Since PI penetrates only within dead cells, the measurement of its fluorescence provided an estimate of the percentage of dead cells. From this estimate, we could deduce the percentage of living cells. In order to measure the fluorescence of PI, the cells were analyzed in a flow cytometer (Beckton Dickinson FACSCalibur 3C), which contains an argon laser with an emission at 488 nm and a FL3-H detector able to detect the fluorescence of PI excited by the laser. Ten thousand cells per sample were measured to determine the percentage of living cells.

**Experimental Protocol Used to Carry Out the *in Vivo* Heating Experiments.** All animal experiments have been conducted after approval of a protocol examined by the committee of the "Centre Léon Bérard, Ecole Normale Supérieure, Plateau de Biologie Expérimentale de la Souris, Lyon, France". *In vivo* heating experiments were carried out on 39 nude mice at 6 weeks of age, which were bought from Charles Rivers Laboratories, Arbresle, France. To prepare tumor-bearing animals, the mice were first gamma-irradiated. Approximately two million MDA MB 231 human breast cancer cells in 100 $\mu$L of PBS were then injected subcutaneously on both the left and right flanks of the mice using a syringe (26G needle). The tumor sizes were measured using calipers every 3 days. The estimates of the volumes of the tumors were then carried out using the formula $V = A \times B^2/2$, where $A$ is the longer and $B$ is the shorter lateral diameter of the tumor. The tumors grew during a period of 21 days until they reached a volume of approximately 100 $mm^3$. Before starting the treatment, the mice were anesthetized with ketamin/xylazin (100/6 mg $kg^{-1}$, ip), which resulted in a decrease of their corporal temperature from 37 °C to 30−36 °C depending on the mouse. Three mice died during the first steps of the treatment most probably due to an overestimation of the dose of anesthetic. After necropsy, the organs of these mice showed no obvious systemic congestion or infarction. Under anesthesia, the needle of the syringe containing the Ch-Std, Ch-EDTA, IM, SPION@Citrate, SPION@PEG, or whole magnetotactic bacteria dispersed in sterile water was inserted longitudinally into the right tumors of the mice as shown in Suppl. Figure 4a. The mice were then placed inside a coil 6.7 cm in diameter, where an alternative magnetic field was applied to them. To produce the alternative magnetic field, an alternative current was generated within the coil using a 10 kW EasyHeat power supply from Ambrell, Soultz, France. The schematic diagram in Suppl. Figure 4b shows the experimental setup used to carry out the treatment induced by heat. The temperature measurements were carried out using an implantable thermocouple microprobe (IT-18, Physitemp, Clifton, USA), specifically adapted to work in the presence of an alternative magnetic field. This thermocouple was used to obtain the rectal temperature or a local estimate of the temperature within the central part of the tumor, as shown in Suppl. Figure 4c. The variation of the rectal temperature was monitored to verify that the increase of the tumor temperature was local and did not affect the whole body temperature of the mice. An infrared camera (Moblr2, Optophase, Lyon, France) was used to obtain a more global picture of the variation of temperature in the tumor and in the tumor environment (Suppl. Figure 4d). The cross section through which the temperature was measured is indicated in Suppl. Figure 4d by a line. The variations of the tumor sizes during the 30 days following the first treatment were measured for both the unheated and heated tumors. Antitumoral activity was studied by following the size evolution of tumors grown subcutaneously on both flanks of each mouse.

**Adjustment of the Strength of the AMF for the Different Groups of Mice.** For the mice that received the suspension containing the Ch-Std or the Ch-EDTA, the magnetic field had to be reduced during the heating cycle (typically by ∼5 mT) to prevent the temperature within the tumor from exceeding 50 °C. For the mice that received the whole inactive magnetotactic bacteria, the magnetic field strength had to be increased to ∼80 mT to yield a detectable temperature increase within the tumor.

**Histological Examinations.** Histological examinations were carried out from subcutaneous samples taken from tumor, liver, kidneys, and lungs collected 30 days after the first injection. Samples were fixed in 10% formalin solution, embedded in paraffin, and sectioned into slices of thickness 4 $\mu$m. The sections were stained with hematoxylin-eosin and with Berlin blue to detect the presence of the bacterial magnetosomes dyed in blue. Necrosis of neoplastic cells, the number of mitoses per three randomly selected fields at a magnification of ×400 in a non-necrotic area, and the amount of pigmented cells were evaluated in pathological sections of the tumors localized on the right flank of the mice.

**Biodistribution Studies: Estimate of the Percentage of Maghemite in the Tumor and Feces.** First, the heating efficiency of the different tumors containing the various types of particles and collected at different days was tested *ex vivo*. For that, the tumor tissue was inserted within a tube, which was then positioned inside a coil where an alternative magnetic field of frequency 183 kHz and field strength of 40 mT was applied during 20 min (EasyHeat 10 kW, Ambrell, Soultz, France). The temperature within the tumor was measured using an implantable thermocouple microprobe (IT-18, Physitemp, Clifton, NJ, USA). Second, the quantity of maghemite was determined using an instrument, the MIAtek, which was developed by the company Magnisense.[40] This technology enables sensitive detection and precise quantification of magnetic nanoparticles in a biological target. For the measurements with the MIAtek, the tissues were prepared by mechanical homogenization in ultrapure water (16% of feces wet weight, *i.e.*, 16 g of feces diluted in 100 mL of PBS, 25% of tumor wet weight, 50% of kidney, lung, spleen wet weight, and 100% liver wet weight). A 100 $\mu$L amount of tissues prepared in this way was placed into the detection system (MIAtek). The calibration was carried out by measuring the MIAtek signal of suspensions containing Ch-Std, IM, SPION@Citrate, and SPION@PEG mixed in water as a function of the maghemite concentration of these suspensions, which was varied between 15 and 125 $\mu$g/mL. In order to verify the estimates of the maghemite concentrations with the MIAtek, SQUID measurements were carried out on the samples containing the highest percentage of maghemite (the tumors and the feces). For that the saturating magnetization of the different tumors and feces containing the various types of particles was estimated. From this estimate, we could deduce the quantity of maghemite present in the different samples using the saturating magnetization of bulk maghemite (80 emu/g). The estimates deduced from the MIAtek measurements have been compared with those deduced from the SQUID measurements. Finally, the different tumors containing the various types of particles were heated *ex vivo* under the application of an alternative magnetic field of frequency 183 kHz and field strength of ∼40 mT. From the heating curves, we could deduce the SAR by measuring their slopes at 25 °C and hence the quantity of maghemite contained within the different tumors. The estimates of the quantity of maghemite contained within the different tumors were obtained by collecting one-fifth of the total tumor volume after homogenization of the particles within the tumors. Most probably because of a non-uniform homogenization, the collected tumor does not contain one-fifth of the amount of the various types of particles injected. This results

in large error bars in the measurements and in some cases in the detection of more particles within the tumor than the amount that was initially injected. However, despite these uncertainties, the main conclusions drawn in this study remain valid.

*Acknowledgment.* We thank Laurence Motte and Yoann Lalatonne for synthesizing the SPION@Citrate and six anonymous reviewers and the editor for their important work on the manuscript, which was thus much improved. Edouard Alphandéry is assistant professor at the University Paris 6. He has set-up a start-up called Nanobacterie in 2008 to develop the therapy of cancer whose proof of concept is presented in this paper. E. A. would like to thank several generous anonymous private investors, Oséo, the so-called "Centre francilien de l'innovation" (Aima Funding), the public French funding program called "Crédit d'impôt recherche", the program Emergence of the UPMC for financial support. We also would like to thank the people who helped us to carry out the experiments at the "Ecole Vétérinaire, Vetagro Sup, 1 avenue Bourgelat, 69280, Marcy L'étoile, France" and at the "Plateau de Biologie Expérimentale de la Souris, PBES, ENS Lyon, 46 allée d'Italie, 69354 Lyon Cedex 7, France."

*Supporting Information Available:* Supplementary Figures 1a, b show optical micrographs of MDA-MB-231 cells incubated in the presence of 1 mg of Ch-Std during 24 h. The Prussian blue coloration indicates the presence of iron within the cells. Suppl. Figure 2a shows the surface charge and the infrared of the IM and Ch-Std as a function of pH. Suppl. Figure 2b shows the absorption spectra of the suspensions of Ch-Std and IM at pH 7. Suppl. Figure 2c shows a TEM image of the SPION@Citrate. Suppl. Figure 3 shows the distributions of magnetosome sizes and magnetosome chain length as well as the heating properties for both the Ch-Std and Ch-EDTA. Suppl. Figure 4 shows several schematic diagrams of the setup used to treat the mice and to measure the temperature within the tumor and rectum. This material is available free of charge *via* the Internet at http://pubs.acs.org.

## REFERENCES AND NOTES

1. See for example a recent study that includes many references about magnetic hyperthermia using magnetic nanoparticles: Rachakatla, R. J.; Balivada, S.; Seo, G.-M.; Myers, C. B.; Wang, H.; Samarakoon, T. N.; Dani, R.; Pyle, M.; Kroh, F. O. Walker, B.; *et al.* Attenuation of Mouse Melanoma by A/C Magnetic Field after Delivery of Bi-Magnetic Nanoparticles by Neural Progenitor Cells. *ACS Nano* **2010**, *4*, 7093–7104.
2. For a review on magnetic hyperthermia see for example: Mornet, S.; Vasseur, S.; Grasset, F.; Duguet, E. Magnetic Nanoparticle Design for Medical Diagnosis and Therapy. *J. Mat. Chem.* **2004**, *14*, 2161–2175.
3. Higler, I.; Andra, W.; Hergt, R.; Hiergeist, R.; Schubert, H.; Kaiser, W. A. Electromagnetic Heating of Breast Tumors in Interventional Radiology: *in vitro* and *in vivo* Studies in Human Cadavers and Mice. *Radiology* **2001**, *218*, 570–575.
4. Ito, A.; Tanaka, K.; Kondo, K.; Shinkai, M.; Honda, H.; Matsumoto, K.; Saida, T.; Kobayashi, T. Tumor Regression by Combined Immunotherapy and Hyperthermia Using Magnetic Nanoparticles in an Experimental Subcutaneous Murine Melanoma. *Cancer Sci.* **2003**, *94*, 308–313.
5. Ito, A.; Tanaka, K.; Honda, H.; Abe, S.; Yamagouchi, H.; Kobayashi, T. Complete Regression of Mouse Mammary Carcinoma with a Size Greater than 15 mm by Frequent Repeated Hyperthermia Using Magnetic Nanoparticles. *J. Biosci. Bioeng.* **2003**, *96*, 364–369.
6. Ito, A.; Kuga, Y.; Honda, H.; Kikkawa, H.; Horiuchi, A.; Watanabe, Kobayashi, T. Magnetic Nanoparticle-loaded anti-HER2 Immunoliposomes for Combination of Antibody Therapy with Hyperthermia. *Cancer Lett.* **2004**, *212*, 167–175.
7. Ito, A.; Honda, H.; Kobayashi, T. Cancer Immunotherapy Based on Intracellular Hyperthermia Using Magnetic Nanoparticles: A Novel Concept of "Heat-Controlled Necrosis" with Heat Shock Protein Expression. *Cancer Immunol. Immun.* **2006**, *55*, 320–328.
8. Maier-Hauff, K.; Rothe, R.; Scholz, R.; Gneveckow, U.; Wust, P.; Thiesen, B.; Feussner, A.; Von Deimling, A.; *et al.* Intracranial Thermotherapy Using Magnetic Nanoparticles Combined with External Beam Radiotherapy: Results of a Feasability Study on Patients with Glioblastoma Multiforme. *J. Neuro-Oncol.* **2007**, *81*, 53–60.
9. Jordan, A.; Scholz, R.; Maier-Hauff, K.; Van Landeghem, F. K. H.; Waldoefner, N.; Teichgraeber, U.; Pinkernelle, J.; Bruhn, H.; Neumann, F.; Thiesen, B.; *et al*. The Effect of Thermotherapy Using Magnetic Nanoparticles on Rat Malignant Glioma. *J. Neuro-Oncol.* **2006**, *78*, 7–14.
10. Johannsen, M.; Gneveckow, U.; Eckelt, L.; Feussner, A.; Waldofner, N.; Scholz, R.; Deger, S.; Wust, P.; Loening, S. A.; Jordan, A. Clinical Hyperthermia of Prostate Cancer Using Magnetic Nanoparticles: Presentation of a New Interstitial Technique. *Int. J. Hyperthermia* **2005**, *21*, 637–647.
11. Johannsen, M.; Gnevekow, U.; Thisen, B.; Taymoorian, K.; Cho, C. H.; Waldofner, N.; Scholz, R.; Jordan, A.; Loening, S. A.; Wust, P. Thermotherapy of Prostate Cancer Using Magnetic Nanoparticles: Feasability, Imaging, and Three-Dimensional Temperature Distribution. *Int. J. Hyperthermia* **2007**, *52*, 1653–1662.
12. Kawai, N.; Ito, A.; Nakahara, Y.; Futakuchi, M.; Shirai, T.; Honda, H.; Kobayashi, T.; Kohri, K. Anticancer Effect of Hyperthermia on Prostate Cancer Meditated by Magnetite Cationic Liposomes and Immune Response Induction in Transplanted Syngeneic Rats. *The Prostate* **2005**, *64*, 373–381.
13. Kawai, N.; Ito, A.; Futakuchi, Yoshida, T.; Ito, A.; Sato, S.; Naiki, T.; M.; Honda, H.; Shirai, T.; Kohri, K. Effect of Heat Therapy Using Magnetic Nanoparticles Conjugated With Cationic Liposomes on Prostate Tumor in Bone. *The Prostate* **2008**, *68*, 784–792.
14. DeNardo, S. J.; De Nardo, G. L.; Miers, L. A.; Natarajan, A.; Foreman, A. R.; Gruettner, C.; Adamson, G. N.; Ivkov, R. Development of Tumor Targeting Bioprobes ($^{111}$In-Chimeric L6Monoclonal Antibody Nanoparticles) for Alternating Magnetic Field Cancer Therapy. *Clin. Cancer Res.* **2005**, *11*, 7087s–7092s.
15. DeNardo, S. J.; De Nardo, G. L.; Natarajan, A.; Miers, L. A.; Foreman, A. R.; Gruettner, C.; Grete, N.; Adamson, G. N.; Ivkov, R. Thermal Dosimetry Predictive of Efficacy of 111In-ChL6 Nanoparticle AMF-Induced Thermoablative Therapy for Human Breast Cancer in Mice. *J. Nucl. Med.* **2007**, *48*, 437–444.
16. Kikumori, T.; Kobayashi, T.; Sawaki, M.; Imai, T. Anti-Cancer Effect of Hyperthermia on Breast Cancer by Magnetite Nanoparticle-Loaded anti-HER2 Immunoliposomes. *Breast Cancer Res. Treat.* **2009**, *113*, 435–441.
17. These companies are Sirtex (an Australian company), Magforce (a German company), and Aspen Medisys (an American company, previously Aduro Biotech and Triton Biosystem).
18. The patents submitted by the companies mentioned in ref 17 are for Sirtex US2006167313 or WO 2004/064921, for Triton Biosystems now Aspen Medisys, LLC: US2003/0028071, and for Magforce , US2008/0268061.
19. Alphandéry, E.; Faure, S.; Raison, L.; Duguet, E.; Howse, P. A.; Bazylinski, D. A. Heat Production by Bacterial Magnetosomes Exposed to an Oscillating Magnetic Field. *J. Phys. Chem. C* **2011**, *115*, 18–22.
20. Hergt, R.; Dutz, S.; Muller, R.; Zeisberger, M. Magnetic Particle Hyperthermia: Nanoparticle Magnetism and Materials Development for Cancer Therapy. *J. Phys.: Condens. Matter* **2006**, *18*, S2919–S2934.
21. Bazylinski, D. A.; Frankel, R. B. Magnetosome Formation in Prokaryotes. *Nat. Rev. Microbiol.* **2004**, *2*, 217–230.
22. Arakaki, A.; Nakazawa, H.; Nemoto, M.; Mori, T.; Matsunaga, T. Formation of Magnetite by Bacteria and its Application. *J. R. Soc. Interface* **2005**, *5*, 977–999.
23. Hergt, R.; Hiergeist, R.; Zeisberger, M.; Schüler, D.; Heyen, U.; Hilger, I.; Kaiser, W. A. Magnetic Properties of Bacterial Magnetosomes as Potential Diagnostic and Therapeutical Tools. *J. Magn. Magn. Mater.* **2005**, *293*, 80–86.
24. Timko, M.; Dzarova, A.; Kovac, J.; Skumiel, A.; Józefczak, A.; Hornowski, T.; Gojz ewski, H.; Zavisova, V.; Koneracka, M.; Sprincova, A.; *et al.* Magnetic Properties and Heating Effect in Bacterial Magnetic Nanoparticles. *J. Magn. Magn. Mat.* **2009**, *321*, 1521–1524.

25. Sun, J.-B.; Wang, Z.-L.; Duan, J.-H.; Ren, J.; Yang, X.-D.; Dai, S.-L.; Li, Y. Targeted Distribution of Bacterial Magnetosomes from *Magnetospirillum gryphiswaldense* MSR-1 in Healthy Sprague-Dawley Rats. *J. Nanosci. Nanotechnol.* **2009**, *9*, 1881–1885.
26. Sun, J.; Tang, T.; Duan, J.; Xu, P.-X.; Wang, Z.; Zhang, Y.; Wu, L.; Li, Y. Biocompatibility of Bacterial Magnetosomes: Acute Toxicity, Immunotoxicity and Cytotoxicity. *Nanotoxicology* **2010**, *4*, 271–283.
27. SPION stabilized by molecules, which are not antitumoral, such as citrate, are used by the group of Jordan (refs 8, 9, 10, 11). The same types of SPION but encapsulated within magneto cationic liposomes are used by the group of Ito (refs 4, 5, 6, 7). SPION stabilized by PEG molecules and available commercially from Micromod are used by the group of De Nardo (refs 14 and 15).
28. Scheffel, A.; Gruska, M.; Faivre, D.; Linaroudis, A.; Plitzko, J. M.; Schüler, D. An Acidic Protein Aligns Magnetosomes Along a Filamentous Structure in Magnetotactic Bacteria. *Nature* **2006**, *440*, 110–114.
29. Alphandéry, E.; Ding, Y.; Ngo, A. T.; Wang, Z. L.; Pileni, M. P. Assemblies of Aligned Magnetotactic Bacteria and Extraced Magnetosomes: What Is the Main Factor Responsible for the Magnetic Anisotropy? *ACS Nano* **2009**, *3*, 1539–1547.
30. Alphandéry, E.; Ngo, A. T.; Lefèvre, C.; Liesiecki, I.; Wu, L. F.; Pileni, M. P. Difference between the Magnetic Properties of the Magnetotactic Bacteria and those of the Extracted Magnetosomes: Influence of the distance between the Chains of Magnetosomes. *J. Phys. Chem. C* **2008**, *112*, 12304–12309.
31. Hui, C.; Shen, C.; Yang, T.; Bao, L.; Tian, J.; Ding, H.; Li, C.; Gao, H.-G. Large Scale $Fe_3O_4$ Nanoparticles Soluble in Water Synthesized by a Facile Method. *J. Phys. Chem. C* **2008**, *112*, 11336–11339.
32. Liu, D.; Wu, W.; Ling, J.; Wen, S.; Gu, N.; Zhang, X. Effective PEGylation of Iron Oxide Nanoparticles for High Performance In Vivo Cancer Imaging. *Adv. Funct. Mater.* **2011**, *21*, 1498–1504.
33. Ivkov, R.; DeNardo, S. J.; Daum, W.; Foreman, A. R.; Goldstein, C. G.; Nemkov, V. S.; DeNardo, G. L. Application of High Amplitude Alternative Magnetic Fields for Heat Induction of Nanoparticles Localized in Cancer. *Clin. Cancer Res.* **2005**, *11*, 7093s–7103s.
34. The optimum conditions of the therapy correspond to those that yield a low toxicity or a low percentage of inhibition in the presence of the AMF or Ch-Std used individually and a high toxicity or high percentage of inhibition in the presence of both the AMF and the Ch-Std.
35. This behavior is clarified by the *in vivo* experiments, which show a high percentage of penetration of iron within the cells (Figure 5d).
36. When 2 mg of SPION@Citrate is administered within the xeno-grafted tumors of a group of six mice and the nanoparticles are heated by applying the AMF, we observe the complete disappearance of the tumor in one mouse, indicating that magnetic hyperthermia can be carried out using SPION. However, in the latter case, it requires the use of a larger amount of material than that necessary if one uses Ch-Std or Ch-EDTA.
37. Puntarulo, S. Iron Oxidative Stress and Human Health. *Mol. Aspects Med.* **2005**, *26*, 299–312.
38. Lalatonne, Y.; Motte, L.; Richardi, Y.; Pileni, M.-P. Influence of Short-Range Interactions on the Mesoscopic Organization of Magnetic Nanocrystals. *Phys. Rev. E* **2005**, *71*, 011404-1–101140410-10.
39. Mosmann, T. Rapid Colorimetric Assay for Cellular Growth and Survival: Application to Proliferation and Cytotoxicity Assays. *J. Immunol. Methods* **1983**, *65*, 55–63.
40. Nikitin, P. I.; Vetoshko, P. M.; Ksenevich, T. I. New Type of Biosensor Based on Magnetic Nanoparticle Detection. *J. Magn. Mater.* **2007**, *311*, 445–449.